


## Stress Isotropization in Weakly Jammed Granular Packings

Félix Benoist<sup>1,2</sup>, Mehdi Bouzid,<sup>3</sup> and Martin Lenz<sup>1,4,\*</sup><sup>1</sup>Université Paris-Saclay, CNRS, LPTMS, 91400, Orsay, France<sup>2</sup>Gulbenkian Institute of Molecular Medicine, Oeiras, Portugal<sup>3</sup>Université Grenoble Alpes, CNRS, Grenoble INP, 3SR, 38000 Grenoble, France<sup>4</sup>PMMH, CNRS, ESPCI Paris, PSL University, Sorbonne Université, Université de Paris, F-75005, Paris, France (Received 30 September 2024; revised 26 April 2025; accepted 9 December 2025; published 22 December 2025)

When sheared, granular media experience localized plastic events known as shear transformations, which generate anisotropic internal stresses. Under strong confining pressure, the response of granular media to local force multipoles is essentially linear, resulting in quadrupolar propagated stresses. This can lead to additional plastic events along the direction of the increase in relative stress. Closer to the unjamming transition, however, as the confining pressure and the shear modulus vanish, nonlinearities become relevant. Yet, the consequences of these nonlinearities on the stress response to plastic events remain poorly understood. We show with granular dynamics simulations that this brings about an isotropization of the propagated stresses, in agreement with a previously developed continuum elastic model. This could significantly modify the yielding transition of weakly jammed amorphous media, which has been conceptualized as an avalanche of such plastic events.

DOI: 10.1103/1psy-gs1v

**Introduction**—When subjected to large enough macroscopic shear stress, amorphous solids such as granular packings, foams, metallic glasses, or toothpaste start to flow [1,2]. This yielding transition originates in microscopic events where the material locally undergoes a plastic deformation [3]. Each of these so-called shear transformations induces new microscopic stresses in its surroundings, which can then trigger further shear transformations. Above a critical macroscopic stress, the catastrophic accumulation of such events is widely believed to cause the whole material to yield and transition from a solidlike to a fluidlike behavior [4].

This yielding transition has been widely studied via mesoscopic elastoplastic models [1,5–10]. Its universality class depends on the propagator, which determines how a shear transformation redistributes stress. Linear elastic solids display a so-called Eshelby propagator, whose quadrupolar symmetry imposes a balance of positive and negative stresses [11,12]. This symmetry, associated with the dipolar deformation field illustrated in Figs. 1(a) and 1(b), dictates the critical exponents at the yielding transition. Among them, the Herschel-Bulkley exponent describes how abruptly the material starts to flow once the macroscopic stress exceeds its critical value [7,13]. Phenomena such as shear banding and aging have also been linked to the form of the Eshelby propagator [14–16].

Although the validity of the Eshelby propagator is well established in dense amorphous solids [19], looser

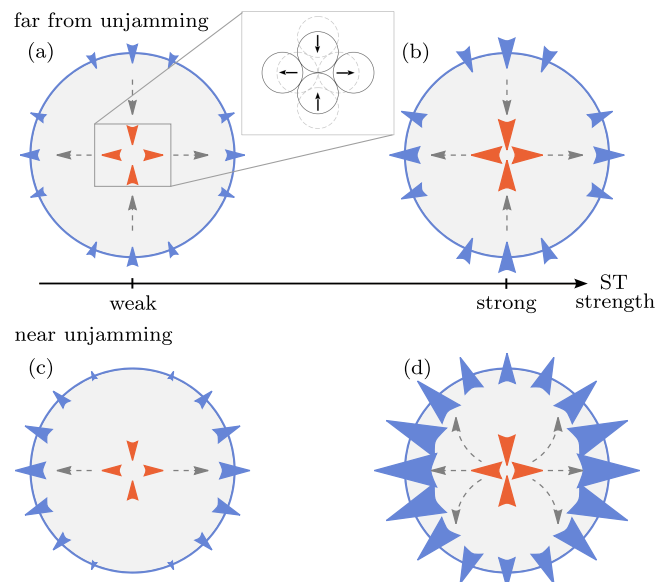


FIG. 1. The far-field stresses induced by a shear transformation (ST) become more isotropic near unjamming. (a) In an amorphous medium, a shear transformation, e.g., a local change of neighbors between grains (inset) [17,18], applies a local force dipole (orange arrowheads) on the surrounding medium. These forces propagate through the medium (gray arrows), resulting in stresses at the medium's boundary (blue arrowheads). (b) Far from unjamming, the medium propagates stresses according to linear elasticity. The symmetry of this stress response is thus independent of the magnitude of the local forces. (c) Close to unjamming, the medium may not support the propagation of tensile stresses, resulting in a dilational stress response. (d) For large local forces, stress redistribution within the medium results in an increasingly isotropic dilation.

\*Contact author: martin.lenz@cnrs.fr

packings may display more complex responses. Experiments on weakly jammed emulsions [20,21] thus indicate a non-Eshelby propagation whereby the change in local stress surrounding a shear transformation has the same sign in all directions [18]. Similarly, an isotropic core is observed in the displacement response to force dipoles of simulated harmonic sphere packings near unjamming [22]. In this Letter, we propose that such deviations from the Eshelby propagator are generically expected for amorphous solids close to unjamming.

Our approach is based on the observation that as an isotropic material approaches unjamming, one or both elastic moduli vanish, while its higher-order nonlinear elastic response remains finite [23–25], leading to a nonlinear response to local shear transformations. To understand the origin of this nonlinearity, consider two contacting grains within the medium. Compressive forces maintain contact, whereas tensile forces tend to pull the grains apart, favoring the transmission of compressive over tensile stresses. As a result, local forcing induces a bias toward isotropic dilation [Figs. 1(c) and 1(d)], an effect that we have previously termed rectification [26,27]. Here, we validate this isotropization using numerical simulations of 2D granular packings. We find that the system’s tendency to isotropization diverges as unjamming is approached, in agreement with a nonlinear elastic model [27]. Finally, a simple toy model suggests that this effect can alter critical exponents and qualitative features of the yielding transition in amorphous solids near unjamming.

*Stress propagation around a shear transformation near unjamming*—We consider packings of frictionless, bidisperse disks confined within a circular arena of radius  $r_{\text{out}}$ , at mechanical equilibrium, as described in the End Matter. The two disk species are present in equal proportions, with a diameter ratio of 1.4. We use the mean diameter as our length unit. The disk area fraction  $\phi$  is set slightly above the critical value  $\phi_c \simeq 0.84$  at which the packing unjams [23], such that  $\Delta\phi = \phi - \phi_c \lesssim 0.2$ . A pair of disks with overlap  $\delta$  interacts elastically via a Hertzian potential proportional to  $\delta^{5/2}$  [28]. The associated stiffness sets our unit of stress. For the values of  $\phi$  considered here, the resulting initial pressure is low, with  $P_{\text{init}} \lesssim 0.02$ . To mimic stress propagation around a shear transformation, we apply internal forces at a radius  $r_{\text{in}}$  [Fig. 2(a)]. In practice, we use mesoscopic values for  $r_{\text{in}}$  to mitigate fluctuations due to the medium’s disorder, and we apply forces on the order of, or smaller than,  $P_{\text{init}}$  to avoid triggering extensive plastic reorganizations [10].

We characterize the magnitude and anisotropy of these forces through the corresponding coarse-grained local stress tensor  $\bar{\sigma}^l$  (definition in End Matter). We monitor stress propagation via the boundary stress response tensor  $\bar{\sigma}^b$ , which characterizes the forces exerted by the medium at its boundary in response to  $\bar{\sigma}^l$ . Our local forcing is decomposed into an isotropic pressure  $\mathcal{P}_l$  and a shear stress  $\mathcal{S}_l$ ,

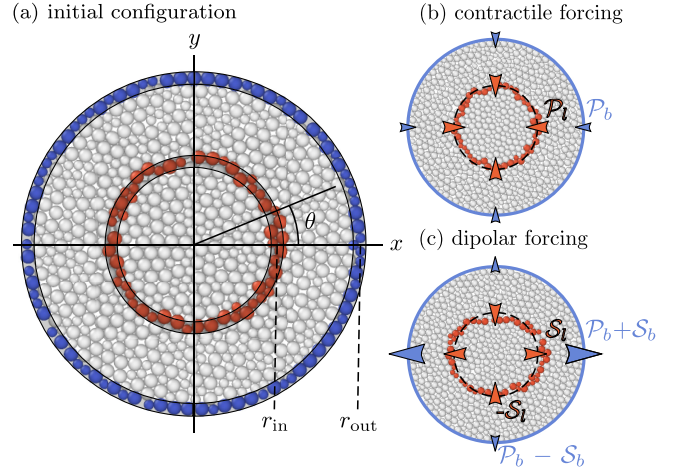


FIG. 2. We subject circular jammed packings to small internal forces. (a) Packing of the type used in our simulations but with fewer disks. We exert radial forces on the disks in the shaded region near  $r_{\text{in}}$  (orange) and measure the forces exerted on the disks in the shaded region near  $r_{\text{out}}$  (blue). (b) The same packing under isotropic contractile forcing,  $\mathcal{P}_l < 0$ , corresponding to a local shrinkage of the original orange ring. In the final configuration, some gray disks are now subject to the forcing, and some orange ones are not. The dashed circle has radius  $r_{\text{in}}$ . (c) Dipolar forcing,  $\mathcal{S}_l > 0$ .

respectively illustrated in Figs. 2(b) and 2(c). We decompose  $\bar{\sigma}^b$  similarly. Placing ourselves in the eigenbasis of tensor  $\bar{\sigma}^l$ , we write

$$\bar{\sigma}^i = - \begin{pmatrix} \mathcal{P}_i + \mathcal{S}_i & 0 \\ 0 & \mathcal{P}_i - \mathcal{S}_i \end{pmatrix} \quad (1)$$

for  $i \in \{l, b\}$ . Qualitatively, a positive  $\mathcal{P}_b$  corresponds to an overall dilation of the medium. Note that for an individual realization of our granular packing, the off-diagonal components of  $\bar{\sigma}^b$  in Eq. (1) may not vanish. Symmetry, however, imposes that their average over the disorder does, and in practice, the off-diagonal components do not exceed 10% of the diagonal ones for any of our individual packings.

In the initial configurations, the confining pressure elicits an isotropic arrangement of force chains; see Fig. S1 in [29]. The application of a dipolar forcing  $\mathcal{S}_l > 0$  rearranges the force chains anisotropically, as shown in Figs. 3(a), S2, and S3. We focus on the outer region,  $r > r_{\text{in}} + \frac{1}{2}$ , through which the local forcing propagates to the boundary. As  $\mathcal{S}_l$  increases and nonlinearities become prevalent, the force chains in the vicinity of the  $y$ -axis near radius  $r_{\text{in}}$  become weaker. Conversely, the force chains near the  $x$ -axis are reinforced, both horizontally and along directions with significant angles with the  $x$ -axis. At large values of  $r$ , this anisotropic propagation leads to reinforced force chains even close to the  $y$ -axis. As a result, a dilational boundary pressure  $\mathcal{P}_b > 0$  emerges in response to the local shear stress  $\mathcal{S}_l$  [Figs. 3(b) and S4]. In extreme cases, this can rectify the stress response toward dilation in all directions,

thus making it more isotropic; see Fig. 3(c). Under isotropic forcing  $\mathcal{P}_l \neq 0$ , we also observe nonlinear relationships between  $\mathcal{P}_b$  and  $\mathcal{P}_l$  (Figs. S5, S6). Overall, this minimal new setup clearly shows how microscopic force chain rearrangements induce the isotropization of propagated stresses illustrated in Fig. 1.

*Dependence of the non-Eshelby propagation on material behavior*—To assess the relationship between isotropization and unjamming, we now turn to theory. Within the linear regime, homogeneous elastic media propagate stress without alteration, such that  $\mathcal{P}_b = \mathcal{P}_l$  and  $\mathcal{S}_b = \mathcal{S}_l$ . For weak nonlinearities, symmetries dictate

$$\mathcal{P}_b \sim \mathcal{P}_l + \alpha \mathcal{S}_l^2 + \beta \mathcal{P}_l^2 \quad \text{and} \quad \mathcal{S}_b \propto \mathcal{S}_l. \quad (2)$$

The term  $\alpha \mathcal{S}_l^2$ , if large and positive, induces dilational stresses that come to dominate the medium's response, and it is, thus, responsible for isotropization. In a previous paper [27], we expressed  $\alpha$  as a function of the material's elastic properties. To parametrize those, we consider a jammed disk packing initially at area fraction  $\phi_0 = \phi_c + \Delta\phi$  with differential bulk and shear moduli  $\kappa_0$  and  $\mu_0$ . When subjected to a small additional compression  $\delta\phi \ll \Delta\phi$ , its moduli become, to first order in  $\delta\phi$ ,

$$\kappa = \kappa_0 \left( 1 - \kappa_1 \frac{\delta\phi}{\phi_c} \right) \quad \text{and} \quad \mu = \mu_0 \left( 1 - \mu_1 \frac{\delta\phi}{\phi_c} \right). \quad (3)$$

The isotropization coefficient  $\alpha$  then reads

$$\alpha = -\frac{1}{\mu_0} \left[ \left( \kappa_1 + \frac{3}{2} \right) \alpha_1 + \left( \mu_1 + \frac{3}{2} \right) \alpha_2 \right], \quad (4)$$

where  $\alpha_1$  and  $\alpha_2$  are positive functions of the ratio of radii  $r_{\text{out}}/r_{\text{in}}$  and Poisson's ratio  $\nu = (\kappa_0 - \mu_0)/(\kappa_0 + \mu_0)$ ; see End Matter for full expressions.

For granular materials under Hertzian interactions, the bulk and shear moduli vanish at unjamming as  $\kappa \sim \kappa_0 \approx \sqrt{\Delta\phi}$  and  $\mu \sim \mu_0 \approx \Delta\phi$  [23]. Expanding the expressions of  $\kappa$  and  $\mu$  for small  $\delta\phi$  and equating the result to Eq. (3) yields

$$\kappa_1 \underset{\Delta\phi \rightarrow 0}{\sim} -\frac{1}{2} \frac{\phi_c}{\Delta\phi} \quad \text{and} \quad \mu_1 \underset{\Delta\phi \rightarrow 0}{\sim} -\frac{\phi_c}{\Delta\phi}. \quad (5)$$

Therefore,  $\kappa_1$  and  $\mu_1$  are both negative. Granular media indeed soften under tension ( $\delta\phi < 0$ ) and stiffen under compression. These nonlinear coefficients, moreover, diverge near unjamming as  $(\Delta\phi)^{-1}$ , leading to a large positive isotropization coefficient  $\alpha$ ; see End Matter. According to Eq. (2), an anisotropic forcing already gives rise to a significantly isotropized far-field stress response (i.e.,  $\mathcal{P}_b > \mathcal{S}_b$ ) for a small  $\mathcal{S}_l \approx \alpha^{-1} \approx (\Delta\phi)^2$ .

To confirm this predominance of isotropization in the vicinity of unjamming, we measure coefficients  $\alpha$  and  $\beta$  in simulations of the type of those presented in Fig. 3 for

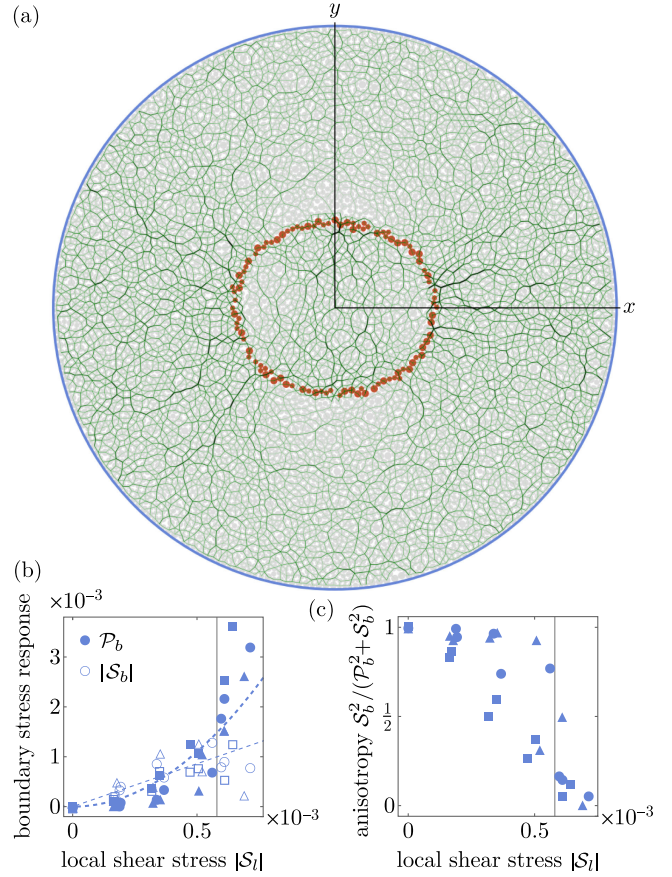


FIG. 3. Force chains rearrange to create boundary dilation out of local shear stress. (a) Local shear stress rearranges force chains in a packing. The green segments have widths and colors proportional to the forces between neighboring disks. We refer to consecutive segments with large widths as force chains. Here, we have  $\approx 6700$  disks,  $r_{\text{out}} \approx 44$ ,  $r_{\text{out}}/r_{\text{in}} = 3$ ,  $\Delta\phi \approx 0.03$ . (b) Dilation under dipolar forcing for three initial configurations (circles, squares, and triangles), demonstrating reproducibility. We fit the data using  $\mathcal{P}_b = \alpha \mathcal{S}_l^2$  with  $\alpha \approx 4400$ , and  $\mathcal{S}_b = (1 + B)\mathcal{S}_l$  with  $B \approx 0.7$ . Here,  $r_{\text{out}}/r_{\text{in}} = 8$ ,  $r_{\text{in}} \approx 5.5$ ,  $\Delta\phi \approx 0.03$ . (c) The anisotropy in the stress response decreases as the local shear stress increases. The vertical line indicates the local shear stress at which this anisotropy falls under 1/2.

different values of  $\Delta\phi$  and  $r_{\text{in}}$  (additional fits in Figs. S4–S9) and report them in Fig. 4. We find that the small nonlinearity expansion of Eq. (2) describes our data well even in regimes where the nonlinear terms are comparable to or larger than the linear ones. We observe an unexpected steeper linear dependence  $\mathcal{S}_b = (1 + B)\mathcal{S}_l$  than predicted, but find that the phenomenological coefficient  $B > 0$  is not large enough to prevent isotropic dilation from dominating the response of our packings (insets of Fig. 4). Both coefficients  $\alpha$  and  $\beta$  are positive, and thus contribute to the medium's dilation in the nonlinear regime. This dilation is, moreover, strongest for small  $\Delta\phi$  and for a very localized forcing ( $r_{\text{in}}$  small). Finally, we compare the values of the main isotropization coefficient

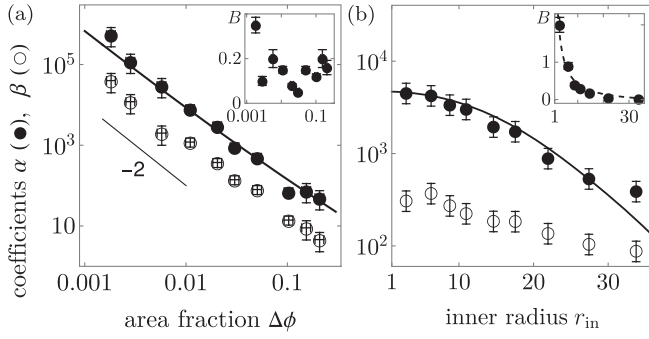


FIG. 4. Isotropization prevails close to unjamming and in large systems. (a) Log-log plot of coefficients  $\alpha$  and  $\beta$  obtained as in the fits of Fig. 3(b) showing a  $(\Delta\phi)^{-2}$  divergence as unjamming is approached. The black line shows our theoretical predictions [Eq. (4)], and we observe  $\beta \simeq \alpha/9$ . Inset: the phenomenological coefficient  $B$  does not strongly depend on  $\Delta\phi$ . Here,  $r_{\text{in}} \simeq 22$  and  $r_{\text{out}} \simeq 44$ . (b) Holding the outer radius  $r_{\text{out}} \simeq 44$  constant, the isotropization coefficient  $\alpha$  is strongest for small  $r_{\text{in}}$ , in agreement with the theoretical prediction (see End Matter). Inset:  $B$  is also large for small  $r_{\text{in}}$ ; the dashed line shows a heuristic dependence  $B = (r_{\text{out}}/r_{\text{in}} - 1)/8$ . Here,  $\Delta\phi \simeq 0.03$ . Bars show standard deviation across three simulations.

$\alpha$  with the prediction of Eqs. (4) and (5). We find a very good agreement without any adjustable parameters (we obtain  $\kappa_0$  and  $\mu_0$  from Ref. [23]), confirming that close to unjamming, the weakening of the packing's linear response induces an overwhelmingly dilational, non-Eshelby response to localized forces.

*Macroscopic implications of the non-Eshelby propagation*—In amorphous solids, shear transformations can trigger further plastic events via stress propagation. In elastoplastic models, this cascade is governed by the Eshelby propagator's quadrupolar symmetry, which makes a shear transformation equally likely to promote or suppress plastic reorganizations in nearby regions. Loosely defining a scalar stress  $\sigma$  characterizing how far a region is from the reorganization threshold  $\sigma_c$ , this implies that  $\sigma$  undergoes a symmetric random walk prior to reaching  $\sigma_c$ . By contrast, Eq. (2) predicts an additional dilational stress  $\mathcal{P}_b$ , which should bias this walk and alter the universality of the fluidization transition.

To illustrate the macroscopic implications of this breaking of the stress-reversal symmetry, we turn to a simple mean-field elastoplastic model [5] that monitors the probability density  $P(\sigma, t)$  of local stresses over time  $t$ . In a material under external shear at rate  $\dot{\gamma}$ ,  $\sigma$  increases at rate  $\mu\dot{\gamma}$ . It also diffuses due to stress kicks from distant shear transformations, with diffusion coefficient  $D = a\Gamma$ , where  $\Gamma$  is the number of plastic reorganizations per unit time, and  $a$  is a constant. We reason that the added dilational stress  $\mathcal{P}_b$  increases the packing pressure, and thus, reduces the tendency to yield [2]. At leading order, this introduces a drift away from the yielding threshold that is proportional to  $\Gamma$ . It can thus be represented by adding a current  $-bD$  to

the evolution equation for  $P(\sigma, t)$ , where  $b$  is a constant:

$$\partial_t P = -(\mu\dot{\gamma} - ba\Gamma)\partial_\sigma P + a\Gamma\partial_\sigma^2 P - \nu(\sigma)P + \Gamma\delta(\sigma). \quad (6)$$

Here, the disappearance rate  $\nu(\sigma) = \tau^{-1}H(|\sigma| - \sigma_c)$ , where  $H$  denotes the Heaviside step function, implies that each region whose stress exceeds the critical value  $\sigma_c$  undergoes a plastic reorganization and is removed from the system. It is then reintroduced as a new stressless configuration through the last term of Eq. (6) involving Dirac's delta function  $\delta$ , with the condition that  $\Gamma(t) = \int_{-\infty}^{+\infty} \nu(\sigma)P(\sigma, t)d\sigma$ . As  $b$  quantifies the relative importance of the dilational and Eshelby stress propagation, we expect it to become relevant close to unjamming.

Analyzing Eq. (6) in a steady state (details in [29]) reveals that just like the classical  $b = 0$  case, our extended  $b \neq 0$  model displays an unjamming transition from a solidlike phase devoid of plastic events at zero shear rate ( $\Gamma = 0$ ) to a fluidlike phase ( $\Gamma \neq 0$ ) upon an increase of  $a$  through a critical value. At the transition, the rheology of the material is described by a Herschel-Bulkley exponent of  $1/2$ :

$$\langle \sigma \rangle - \langle \sigma(\dot{\gamma} = 0) \rangle \approx \dot{\gamma}^{1/2}. \quad (7)$$

By contrast, in the Eshelby-like ( $b = 0$ ) case, this dependence is  $\langle \sigma \rangle \approx \dot{\gamma}^{1/5}$  and only crosses over to a Herschel-Bulkley exponent of  $1/2$  deeper in the jammed phase [30]. While derived in a simplistic model, this indicates that the loss of the Eshelby-like symmetry can have macroscopic implications for the rheology of amorphous materials.

*Discussion*—Our study sheds light on the transmission of internally generated stresses in granular systems close to unjamming. Many elastoplastic models assume that, following a shear transformation, this transmission is well described by an Eshelby-like linear elasticity kernel [1,7,31]. We show that elastic nonlinearities inherent to the unjamming transition instead lead to substantial isotropic dilational stresses around local rearrangements. This isotropization is strongest for rearrangements spanning a few particle diameters, comparable to that of shear transformations [32]. This mirrors earlier experimental [18] and numerical [22] findings.

Although our analysis focuses on Hertzian disk packings, we expect similar results for harmonic interactions (see End Matter) and random spring networks [33,34]. This universal character is reflected in the good agreement between our simulations and a continuum theory devoid of microscopic assumptions; see Ref. [29] for a study of finite-size effects and plasticity (and Refs. [35–41] therein). While based on a small-stress, weakly nonlinear expansion, this formalism quantitatively predicts isotropized stresses even in regimes where they are significantly larger than the stresses predicted by linear elasticity. This is reminiscent of successful predictions of the onset of failure in amorphous solids based on lowest-order nonlinearities

[42]. Crucially, this isotropization requires the vanishing of at least one elastic modulus at unjamming. Systems where  $K$  and  $G$  remain finite at the transition should, thus, display negligible far-field stress isotropization.

We use an elastoplastic toy model to bring out the macroscopic consequences of the isotropization-induced breaking of symmetry between positive and negative stresses. Consistent with recent non-mean-field results, we find that this asymmetry changes the characteristics of the unjamming transition [43]. Moreover, while yielding in strongly jammed systems tends to concentrate along transient slip lines [14,44,45], we predict more homogeneous, ductilelike yielding in weakly jammed systems due to more isotropic propagated stresses [15,46].

*Acknowledgments*—M. L. and F. B. thank Éric Clément and Sylvain Patinet for fruitful discussions. M. L. was supported by Marie Curie Integration Grants No. PCIG12-GA-2012-334053, “Investissements d’Avenir” LabEx PALM (No. ANR-10-LABX-0039-PALM), No. ANR-21-CE11-0004-02, No. ANR-22-ERCC-0004-01, and No. ANR-22-CE30-0024-01, as well as ERC Starting Grant No. 677532 and the Impulscience program of Fondation Bettencourt-Schueller. M. L.’s group belongs to the CNRS consortium AQP.

- 
- [1] A. Nicolas, E. E. Ferrero, K. Martens, and J.-L. Barrat, Deformation and flow of amorphous solids: Insights from elastoplastic models, *Rev. Mod. Phys.* **90**, 045006 (2018).
- [2] D. Bonn, M. M. Denn, L. Berthier, T. Divoux, and S. Manneville, Yield stress materials in soft condensed matter, *Rev. Mod. Phys.* **89**, 035005 (2017).
- [3] A. Argon, Plastic deformation in metallic glasses, *Acta Metall.* **27**, 47 (1979).
- [4] T. Divoux *et al.*, Ductile-to-brittle transition and yielding in soft amorphous materials: Perspectives and open questions, *Soft Matter* **20**, 6868 (2024).
- [5] P. Hébraud and F. Lequeux, Mode-coupling theory for the pasty rheology of soft glassy materials, *Phys. Rev. Lett.* **81**, 2934 (1998).
- [6] L. Bocquet, A. Colin, and A. Ajdari, Kinetic theory of plastic flow in soft glassy materials, *Phys. Rev. Lett.* **103**, 036001 (2009).
- [7] J. Lin, E. Lerner, A. Rosso, and M. Wyart, Scaling description of the yielding transition in soft amorphous solids at zero temperature, *Proc. Natl. Acad. Sci. U.S.A.* **111**, 14382 (2014).
- [8] Z. Budrikis, D. F. Castellanos, S. Sandfeld, M. Zaiser, and S. Zapperi, Universal features of amorphous plasticity, *Nat. Commun.* **8**, 15928 (2017).
- [9] M. Talamali, V. Petäjä, D. Vandembroucq, and S. Roux, Avalanches, precursors, and finite-size fluctuations in a mesoscopic model of amorphous plasticity, *Phys. Rev. E* **84**, 016115 (2011).
- [10] M. Bouzid, A. Izzet, M. Trulsson, E. Clément, P. Claudin, and B. Andreotti, Non-local rheology in dense granular flows, *Eur. Phys. J. E* **38**, 125 (2015).
- [11] J. D. Eshelby, The determination of the elastic field of an ellipsoidal inclusion, and related problems, *Proc. R. Soc. A: Math. Phys. Eng. Sci.* **241**, 376 (1957).
- [12] K. Karimi and J.-L. Barrat, Correlation and shear bands in a plastically deformed granular medium, *Sci. Rep.* **8**, 4021 (2018).
- [13] J. Lin, A. Saade, E. Lerner, A. Rosso, and M. Wyart, On the density of shear transformations in amorphous solids, *Europhys. Lett.* **105**, 26003 (2014).
- [14] R. Dasgupta, H. G. E. Hentschel, and I. Procaccia, Microscopic mechanism of shear bands in amorphous solids, *Phys. Rev. Lett.* **109**, 255502 (2012).
- [15] B. Tyukodi, S. Patinet, S. Roux, and D. Vandembroucq, From depinning transition to plastic yielding of amorphous media: A soft-modes perspective, *Phys. Rev. E* **93**, 063005 (2016).
- [16] K. Martens, L. Bocquet, and J.-L. Barrat, Spontaneous formation of permanent shear bands in a mesoscopic model of flowing disordered matter, *Soft Matter* **8**, 4197 (2012).
- [17] A. Kabla and G. Debrégeas, Local stress relaxation and shear banding in a dry foam under shear, *Phys. Rev. Lett.* **90**, 258303 (2003).
- [18] K. W. Desmond and E. R. Weeks, Measurement of stress redistribution in flowing emulsions, *Phys. Rev. Lett.* **115**, 098302 (2015).
- [19] A. Tanguy, F. Leonforte, and J.-L. Barrat, Plastic response of a 2D Lennard-Jones amorphous solid: Detailed analysis of the local rearrangements at very slow strain rate, *Eur. Phys. J. E* **20**, 355 (2006).
- [20] A. J. Liu and S. R. Nagel, Jamming is not just cool any more, *Nature (London)* **396**, 21 (1998).
- [21] M. van Hecke, Jamming of soft particles: Geometry, mechanics, scaling and isostaticity, *J. Phys. Condens. Matter* **22**, 033101 (2009).
- [22] J. A. Giannini, E. Lerner, F. Zamponi, and M. L. Manning, Scaling regimes and fluctuations of observables in computer glasses approaching the unjamming transition, *J. Chem. Phys.* **160**, 034502 (2024).
- [23] C. S. O’Hern, L. E. Silbert, A. J. Liu, and S. R. Nagel, Jamming at zero temperature and zero applied stress: The epitome of disorder, *Phys. Rev. E* **68**, 011306 (2003).
- [24] S. Dagois-Bohy, E. Somfai, B. P. Tighe, and M. van Hecke, Softening and yielding of soft glassy materials, *Soft Matter* **13**, 9036 (2017).
- [25] M. S. van Deen, J. Simon, Z. Zeravcic, S. Dagois-Bohy, B. P. Tighe, and M. van Hecke, Contact changes near jamming, *Phys. Rev. E* **90**, 020202(R) (2014).
- [26] P. Ronceray, C. P. Broedersz, and M. Lenz, Fiber networks amplify active stress, *Proc. Natl. Acad. Sci. U.S.A.* **113**, 2827 (2016).
- [27] F. Benoist, G. Saggiorato, and M. Lenz, Generic stress rectification in nonlinear elastic media, *Soft Matter* **19**, 2970 (2023).
- [28] H. A. Makse, N. Gland, D. L. Johnson, and L. M. Schwartz, Granular packings: Nonlinear elasticity, sound propagation, and collective relaxation dynamics, *Phys. Rev. E* **70**, 061302 (2004).
- [29] See Supplemental Material at <http://link.aps.org/supplemental/10.1103/1psy-gs1v> for additional details.

- [30] E. Agoritsas, E. Bertin, K. Martens, and J.-L. Barrat, On the relevance of disorder in athermal amorphous materials under shear, *Eur. Phys. J. E* **38**, 71 (2015).
- [31] S. Merabia and F. Detcheverry, Thermally activated creep and fluidization in flowing disordered materials, *Europhys. Lett.* **116**, 46003 (2016).
- [32] A. Amon, V. B. Nguyen, A. Bruand, J. Crassous, and E. Clément, Hot spots in an athermal system, *Phys. Rev. Lett.* **108**, 135502 (2012).
- [33] E. Lerner, E. DeGiuli, G. Düring, and M. Wyart, Breakdown of continuum elasticity in amorphous solids, *Soft Matter* **10**, 5085 (2014).
- [34] W. Ellenbroek, Z. Zeravcic, W. Saarloos, and M. van Hecke, Non-affine response: Jammed packings vs. spring networks, *Europhys. Lett.* **87**, 34004 (2009).
- [35] L. E. Silbert, A. J. Liu, and S. R. Nagel, Vibrations and diverging length scales near the unjamming transition, *Phys. Rev. Lett.* **95**, 098301 (2005).
- [36] K. Karimi and C. E. Maloney, Elasticity of frictionless particles near jamming, *Phys. Rev. E* **92**, 022208 (2015).
- [37] W. G. Ellenbroek, M. van Hecke, and W. van Saarloos, Jammed frictionless disks: Connecting local and global response, *Phys. Rev. E* **80**, 061307 (2009).
- [38] M. Wyart, L. E. Silbert, S. R. Nagel, and T. A. Witten, Effects of compression on the vibrational modes of marginally jammed solids, *Phys. Rev. E* **72**, 051306 (2005).
- [39] M. Dinkgreve, J. Paredes, M. A. J. Michels, and D. Bonn, Universal rescaling of flow curves for yield-stress fluids close to jamming, *Phys. Rev. E* **92**, 012305 (2015).
- [40] J. L. Barrat and A. Lemaître, Heterogeneities in amorphous systems under shear, [arXiv:1009.5774](https://arxiv.org/abs/1009.5774).
- [41] C. E. Maloney and M. O. Robbins, Evolution of displacements and strains in sheared amorphous solids, *J. Phys. Condens. Matter* **20**, 244128 (2008).
- [42] S. Karmakar, A. Lemaître, E. Lerner, and I. Procaccia, Predicting plastic flow events in athermal shear-strained amorphous solids, *Phys. Rev. Lett.* **104**, 215502 (2010).
- [43] T. Jocteur, S. Figueiredo, K. Martens, E. Bertin, and R. Mari, Yielding is an absorbing phase transition with vanishing critical fluctuations, *Phys. Rev. Lett.* **132**, 268203 (2024).
- [44] C. E. Maloney and A. Lemaître, Subextensive scaling in the athermal, quasistatic limit of amorphous matter in plastic shear flow, *Phys. Rev. Lett.* **93**, 016001 (2004).
- [45] C. E. Maloney and A. Lemaître, Amorphous systems in athermal, quasistatic shear, *Phys. Rev. E* **74**, 016118 (2006).
- [46] D. Richard *et al.*, Predicting plasticity in disordered solids from structural indicators, *Phys. Rev. Mater.* **4**, 113609 (2020).
- [47] A. P. Thompson *et al.*, LAMMPS—a flexible simulation tool for particle-based materials modeling at the atomic, meso, and continuum scales, *Comput. Phys. Commun.* **271**, 108171 (2022).
- [48] C. F. Schreck, C. S. O’Hern, and L. E. Silbert, Tuning jammed frictionless disk packings from isostatic to hyperstatic, *Phys. Rev. E* **84**, 011305 (2011).

## End Matter

*Appendix A: Simulation methods*—We obtain equilibrated packings by using granular dynamics via LAMMPS [47] version stable\_3Mar2020 as follows. We initialize  $\simeq 6700$  disks with stiffness  $k$  in a random unjammed configuration inside a circular arena ( $k = 1$  in the main text). Two disks of radii  $r_1$  and  $r_2$  with overlap  $\delta$  exert frictionless repulsive forces of magnitude  $k\sqrt{r_1 r_2 / (r_1 + r_2)} \delta^{3/2}$ ; likewise for the disks overlapping with the arena of radius  $r_a = r_{\text{out}} + (D/2)$ , where  $D$  is the mean disk diameter ( $D = 1$  in the main text). The forces  $\{\mathbf{f}^{\nu \rightarrow \mu}\}$  exerted on disk  $\mu$  by its neighbors at positions  $\{\mathbf{r}^\nu\}$  result in an elastic stress, written  $\sigma_{ij}^\mu = -\sum_\nu (r_i^\nu - r_i^\mu) f_j^{\mu \rightarrow \nu}$ . To reach a jammed configuration with packing fraction  $\phi > \phi_c$ , we increase the disk diameters and let the packing relax by thermal annealing [48]. We determine  $\Delta\phi = \phi - \phi_c$  based on the values of the initial pressure after relaxation  $P_{\text{init}}/k \simeq 0.27(\Delta\phi)^{3/2}$  and the excess contact number  $Z_{\text{init}} - 4 \simeq 3.3\sqrt{\Delta\phi}$  [23].

To investigate the response of packings to local forcing, we define an inner ring as  $r \in I_l = [r_{\text{in}} - (D/2), r_{\text{in}} + (D/2)]$  [orange disks in Fig. 2(a)], with area  $A_l = 2\pi r_{\text{in}} D$ . In addition to the forces due to the initial pressure  $P_{\text{init}}$ , we subject each disk  $\mu$  in the inner ring to a constant radial force, written

$$\mathbf{f}^\mu/k = (f_0 + 2f_2 \cos 2\theta^\mu) \hat{\mathbf{r}}^\mu, \quad \text{for } r^\mu \in I_l, \quad (\text{A1})$$

such that  $f_2 = 0$  corresponds to an isotropic forcing [Fig. 2(b)], while  $f_0 = 0$  corresponds to a dipolar forcing [Fig. 2(c)]. This forcing elicits a coarse-grained local stress proportional to the dipole of the added forces:

$$\bar{\sigma}_{ij}^l = \frac{-2D}{A_l} \sum_{\mu \in I_l} f_i^\mu \hat{r}_j^\mu. \quad (\text{A2})$$

We also define a boundary ring as  $r \in I_b = [r_{\text{out}} - (D/2), r_{\text{out}} + (D/2)]$  [blue disks in Fig. 2(a)], with area  $A_b = 2\pi r_{\text{out}} D$ , whose outer part sticks to the arena. The excess stresses on the disks in the boundary ring  $\sigma^\mu - \sigma^{\mu, \text{init}}$  due to the forcing result in a boundary stress response

$$\bar{\sigma}_{ij}^b = \frac{2}{A_b} \frac{r_{\text{out}}^2}{r_{\text{in}}^2} \sum_{k=x,y} \sum_{\mu \in I_b} (\sigma_{ik}^\mu - \sigma_{ik}^{\mu, \text{init}}) \hat{r}_k^\mu \hat{r}_j^\mu. \quad (\text{A3})$$

Due to the ratio  $r_{\text{out}}^2/r_{\text{in}}^2$  compensating for the dilution, the analytical prediction for linear elastic systems is  $\bar{\sigma}^b = \bar{\sigma}^l$  [27]. For moderate forcing,  $f_0, f_2 \lesssim P_{\text{init}}/k$ , the local stress components defined in Eq. (1) increase with forcing as  $P_l \propto f_0$  and  $S_l \propto f_2$ ; see Ref. [29].

*Appendix B: Continuum elastic model*—We previously estimated the isotropization coefficient  $\alpha$  for a continuum elastic medium under internal dipolar forcing [Fig. 2(c)] by expanding Hooke’s law to the lowest nonlinear order [27]. In that framework, nonlinear corrections to the bulk and shear moduli,  $\kappa$  and  $\mu$ , were characterized by the parameters  $\kappa_1$  and  $\mu_1$ . Here, we compute  $\kappa_1$  and  $\mu_1$  directly in granular media and substitute them into the theoretical expression for  $\alpha$  [Eq. (4)] to generate the curves shown in Fig. 4.

We quantify deformation at location  $\mathbf{x}$  using the displacement gradient  $\eta_{ij} = \partial u_i / \partial x_j$ . For small strains, we expand the Cauchy stress  $\boldsymbol{\sigma}$  to the lowest nonlinear order as  $\sigma_{ij} = \mathcal{K}_{ijkl}\eta_{kl} + \mathcal{L}_{ijklmn}\eta_{kl}\eta_{mn}$ . Within this framework, the elastic response of an isotropic and achiral medium to a combination of bulk deformation and simple shear, i.e.,  $\boldsymbol{\eta} = \begin{pmatrix} \eta_{ii}/2 & \eta_{xy} \\ \eta_{xy} & \eta_{ii}/2 \end{pmatrix}$ , is characterized by differential bulk and shear moduli  $\kappa = \partial \sigma_{xx} / \partial \eta_{ii}$ ,  $\mu = \partial \sigma_{xy} / \partial \eta_{xy}$ , written

$$\kappa = \kappa_0(1 + \kappa_1\eta_{ii}) \quad \text{and} \quad \mu = \mu_0(1 + \mu_1\eta_{ii}). \quad (\text{B1})$$

In the setup of Fig. 2, we consider a large packing of frictionless Hertzian disks with area fraction  $\phi_c + \Delta\phi$ . Near unjamming, i.e.,  $0 < \Delta\phi \ll 1$ , the moduli read

$$\kappa = K(\Delta\phi)^s \quad \text{and} \quad \mu = M(\Delta\phi)^t, \quad (\text{B2})$$

where  $K \simeq 0.3$  and  $M \simeq 0.2$  in units of the disk stiffness,  $s \simeq 0.5$  and  $t \simeq 1.0$  [23]. The area fraction  $\phi_c + \Delta\phi$  corresponds to that of a system initially at the rigidity threshold  $\phi_c$  subjected to a bulk compression  $\eta_{ii} = -\eta_0 = -\Delta\phi/\phi_c$ . We then add an even smaller perturbation:  $\eta_{ii} = -\eta_0 - \delta\eta$ , where  $|\delta\eta| \ll \eta_0$  and  $\delta\eta = \delta\phi/\phi_c$ . This results in Eq. (3):

$$\begin{aligned} \kappa &= \kappa_0(1 - \kappa_1\delta\eta) + \mathcal{O}(\delta\eta^2), \\ \mu &= \mu_0(1 - \mu_1\delta\eta) + \mathcal{O}(\delta\eta^2), \end{aligned} \quad (\text{B3})$$

where, at lowest order in  $\Delta\phi$ , the elastic parameters read

$$\begin{aligned} \kappa_0 &= K(\Delta\phi)^s, & \kappa_1 &= -s\phi_c/\Delta\phi, \\ \mu_0 &= M(\Delta\phi)^t, & \mu_1 &= -t\phi_c/\Delta\phi, \end{aligned} \quad (\text{B4})$$

as in Eq. (5). Therefore, given  $\phi_c \simeq 0.84$ , around, e.g.,  $\Delta\phi = 0.1, 0.01$ , or  $0.001$ , we find, respectively,  $\kappa_1 \simeq -4, -40$ , or  $-400$  and  $\mu_1 \simeq -8, -80$ , or  $-800$ . Poisson’s ratio then reads

$$\nu = \frac{\kappa_0 - \mu_0}{\kappa_0 + \mu_0} = 1 - 2\frac{M}{K}(\Delta\phi)^{t-s}. \quad (\text{B5})$$

Thus,  $1 - \nu$  scales approximately as  $(\Delta\phi)^{0.5}$ , such that media far from unjamming are more compressible.

Now that the elastic parameters are properly defined, we enter them into the expression of  $\alpha$  from Ref. [27] reproduced in Eq. (4). Therein,  $\alpha_1$  and  $\alpha_2$  are positive functions of  $\rho = (r_{\text{out}}/r_{\text{in}})^2$  and  $\nu$ , written

$$\begin{aligned} \frac{X\alpha_1}{1 - \nu^2} &= 405 - 108\nu - 54\nu^2 + 12\nu^3 + \nu^4 \\ &+ (324 - 180\nu - 24\nu^2 - 36\nu^3 - 4\nu^4)\rho \\ &+ (378 - 288\nu + 120\nu^2 + 24\nu^3 + 6\nu^4)\rho^2 \\ &+ (108 - 180\nu + 48\nu^2 + 12\nu^3 - 4\nu^4)\rho^3 \\ &+ (81 - 108\nu + 54\nu^2 - 12\nu^3 + \nu^4)\rho^4 \end{aligned}$$

and

$$\begin{aligned} X\alpha_2 &= 81 - 54\nu + 351\nu^2 - 84\nu^3 - 49\nu^4 + 10\nu^5 + \nu^6 \\ &- (684\nu - 204\nu^2 + 120\nu^3 + 8\nu^4 + 28\nu^5 + 4\nu^6)\rho \\ &+ (594 - 900\nu + 1122\nu^2 - 360\nu^3 \\ &+ 102\nu^4 + 12\nu^5 + 6\nu^6)\rho^2 \\ &+ (216 - 1116\nu + 924\nu^2 - 312\nu^3 \\ &+ 16\nu^4 + 20\nu^5 - 4\nu^6)\rho^3 \\ &+ (405 - 702\nu + 567\nu^2 - 276\nu^3 \\ &+ 83\nu^4 - 14\nu^5 + \nu^6)\rho^4, \end{aligned}$$

where

$$X = 4\frac{\rho}{\rho - 1}(3 - \nu)^2[2(3 + \nu) + (3 - \nu)(\rho + \rho^2)]^2.$$

Given the dependencies of the elastic parameters with the area fraction  $\Delta\phi$  in Eq. (B4), approximating  $s$  to 0.5 and  $t$  to 1, we can expand Eq. (4) for small  $\Delta\phi$  as

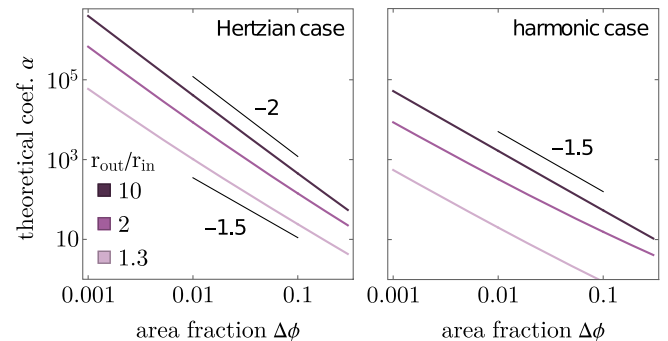


FIG. 5. Theoretical prediction for the isotropization coefficient. Equation (4) predicts different scalings of  $\alpha$  with  $\Delta\phi$  for varying values of  $r_{\text{out}}/r_{\text{in}}$ . For area fractions  $\Delta\phi \in [10^{-3}, 10^{-1}]$ , the exponent varies from  $-2$  when  $r_{\text{out}}/r_{\text{in}} = 10$  to  $-1.5$  when  $r_{\text{out}}/r_{\text{in}} = 1.3$ .

$$\alpha \sim \alpha^{(0)}(\Delta\phi)^{-2} + \alpha^{(1)}(\Delta\phi)^{-3/2}, \quad (\text{B6})$$

where

$$\alpha^{(0)} = \frac{\phi_c}{M} \frac{(\rho-1)^3}{\rho} \frac{4-2\rho+\rho^2}{(4+\rho+\rho^2)^2} t, \quad (\text{B7})$$

$$\alpha^{(1)} = \frac{\phi_c}{K} \frac{\rho-1}{\rho(4+\rho+\rho^2)^3} \left[ 6(\rho-1)^3(8+4\rho+3\rho^2)t + (64+36\rho+81\rho^2+16\rho^3+18\rho^4+\rho^6)s \right]. \quad (\text{B8})$$

Consequently,  $\alpha$  diverges near unjamming as  $(\Delta\phi)^{-2}$ . There is, however, a crossover from a slope  $-2$  to a slope  $-1.5$  at intermediate  $\Delta\phi$ , due to the scaling of  $\nu$  with  $\Delta\phi$  [Eq. (B5)]; see Fig. 5.

For disks interacting with a harmonic potential proportional to  $\delta^2$ , Eq. (B4) has coefficients  $K \simeq 0.3$ ,  $s \simeq 0$ ,  $M \simeq 0.2$ , and  $t \simeq 0.5$  [23]. This translates into

$$\alpha_{\text{har}} \sim \alpha^{(0)}(\Delta\phi)^{-3/2} + \alpha^{(1)}(\Delta\phi)^{-1}, \quad (\text{B9})$$

with identical  $\alpha^{(0)}$ ,  $\alpha^{(1)}$  coefficients. At a given low  $\Delta\phi$ , this yields an isotropization effect that is substantial yet weaker than in the Hertzian case; see Fig. 5.